PEER-REVIEWED ARTICLE

Automatic Detection of Vegetation Changes in the Southwestern United States Using Remotely Sensed Images

Pat S. Chavez, Jr., and David J. MacKinnon

Abstract

The capability to automatically detect vegetation changes using multitemporal remotely sensed image data is of utmost importance to many global-change research projects. A procedure to automatically map vegetation changes within arid and semi-arid regions of the southwestern United States is presented. Multitemporal Landsat Multispectral Scanner (MSS) images were the primary data source, but some preliminary work was also done using same-date Visible-Infrared Spin-Scan Radiometer (VISSR) data for comparison with the MSS results. The change-detection procedure includes multitemporal image calibration using a hybrid method that we developed for the project; the hybrid calibration allows a radiometric calibration to be applied to historical data by using field-radiance information rather than a modeling procedure. The results indicate that a calibrated visible band is more sensitive than the widely used Normalized Difference Vegetation Index (NDVI) in detecting vegetation changes in the arid and semi-arid environments of the southwestern United States. Changes were detected in the desert environment, where the vegetation density is relatively low, with both Landsat MSS and GOES VISSR images. Some changes detected by the automatic procedure were confirmed in the field during two of the Landsat overpasses. The changes corresponded mostly to the blooming of ephemeral or annual vegetation.

Introduction

Digital images obtained through multitemporal satellite remote sensors have been successfully used to map land-cover changes from year to year and season to season (e.g., Shepard, 1964; Robinove *et al.*, 1981; Jensen and Toll, 1982; Fung, 1990). Multitemporal satellite image data have recently become even more important due to their use in research dealing with global change — change occurring both on the surface of the Earth (in its vegetation, land use, etc.) and in its atmosphere. Information about change is used to create models of past and possible future conditions. In this study we are using automatic change-detection techniques and multitemporal image data to correlate vegetation changes with the effects of dust storms. We discussed the detection of dust storms in deserts using images from the NOAA Advanced Very High Resolution Radiometer (AVHRR) and Geostationary Operational Environment Satellite (GOES) Visible-Infrared Spin-Scan Radiometer (VISSR) systems in a previous paper (MacKinnon and Chavez, 1993). The purpose of this paper is to present the automatic change detection procedure, including calibration, and to discuss some of the vegetation change results seen in our study site.

Earth scientists are concerned about dust storms because the storms may indicate that the climate has induced, perhaps irreversible, desertification processes in the source areas of the dust. The most critical results of these storms are the suspension and blowing away as dust of the finest grained soil nutrients, those most capable of assimilation by natural and cultivated plants. Although these nutrients fall mainly into the oceans and can locally nourish oceanic ecosystems, they are permanently removed from land-based ecosystems. The dust also locally degrades air quality and changes the local and global radiation balance, which may eventually trigger other negative climatic effects (Pewe, 1981; UCAR, 1991).

Vegetative cover is the single most effective shield against removal of very small grains of soil by the wind. Consequently, a sensitive method for the detection of vegetative change is essential for determining when the effects of climatic change have substantially degraded these soils. This is one of the main purpose of doing a study such as ours and why change detection is so important. The desert areas that we are presently studying are typical of much larger expanses in the western United States where evidence of catastrophic episodes of climatically induced vegetative changes and subsequent dust storms has been reported (McCauley *et al.*, 1981; Gillette and Hanson, 1989). Because the wind protection offered by vegetation is extremely sensitive to very minor changes in the percentage of cover (Raupach *et al.*, 1993), an essential part of our project involves automatically detecting and mapping these subtle changes, especially over previously defined dust-source areas. In our study we have used mostly multitemporal Landsat Multispectral Scanner (MSS) image data to automatically detect and study the changes in natural vegetation. However, we have done some preliminary work comparing the changes seen in MSS images with changes seen on the same-date GOES VISSR images. The objective of this paper is to present the change-detection procedure and some of the vegetation change results generated using remotely sensed multitemporal images. The procedure

U.S. Geological Survey, 2255 North Gemini Drive, Flagstaff, AZ 86001.

Photogrammetric Engineering & Remote Sensing, Vol. 60, No. 5, May 1994, pp. 571–583.

0099-1112/94/6001–571$03.00/0

includes multitemporal image calibration by a hybrid method developed by merging absolute and relative calibration techniques.

Characteristics of the Data and Test Site

The study area is in the southwestern United States, and Landsat MSS images collected on 4 April 1992, 1 July 1992, 24 February 1981, and 26 February 1984, and GOES VISSR data collected on 4 April 1992 and 1 July 1992 were used. The Landsat MSS images have an approximate spatial resolution of 75 m; the VISSR images have an approximate resolution of 1 km at nadir, similar to AVHRR, and cover a much wider swath than the MSS images. However, the view angle geometry of VISSR images is similar to that of Landsat MSS images rather than AVHRR images because of the much higher altitude of the GOES satellite. The standard false-color composites of the four Landsat MSS images are shown in Plate 1. These images have been geometrically and radiometrically calibrated/slaved onto a master image, and the same contrast stretch was applied to all four for visual display. Because of the radiometric calibration, the brightnesses and colors of the images have the same spectral reflectances if they have the same DN values.

For Yuma, Arizona, which is in the lower part of our study site, the average total yearly precipitation recorded at the National Weather Service station is 63.5 mm. However, in 1992, precipitation for February and March alone was 85.3 mm. Only 10 mm fell in April and May and then nothing through the end of July. Therefore, the 4 April and 1 July 1992 images, respectively, depict the relative surface brightness due to growth of ephemerals at near-peak vigor at the end of the wet season and at complete senescence at the end of the dry season (Plate 2).

The Landsat MSS images of 24 February 1981 and 26 February 1984 (Plate 1) were acquired, respectively, following extremely dry and extremely wet (El Nino) periods spanning much more time than the three months displayed by the 1992 images. From May 1980 through October 1982, the region experienced a severe drought, when only 108.8 mm of precipitation fell in Yuma. The driest portion of that drought was May 1980 through January 1982, when only 38.8 mm of precipitation fell. From November 1982 through January 1983, a total of 84.6 mm of precipitation fell. During the rest of 1983, another 100 mm of precipitation fell. The 1982-83 El Nino was considered the strongest since records were first kept 100 years ago (MacKinnon *et al.*, 1990). Ground photographs taken on 14 January 1984 by these authors confirm that the MSS image acquired on 26 February 1984 shows parts of the desert within our image area with a dramatic bloom in vegetation compared with vegetation imaged on 24 February 1981 when the dry-year Landsat MSS image was acquired.

Besides the satellite images, some photographs were taken on field trips during the 4 April (wet season) and 1 July 1992 (dry season), Landsat MSS overflights and ten days prior to the 4 April overflight (Plate 2). These photographs show the amount of vegetation present in the desert when the image data were recorded. During these field trips, ground-radiance measurements over a bright and dark site were collected for use in the absolute calibration procedure and for checking the accuracy of the calibration models. Exotech model 100-AX radiometers with spectral filters corresponding to the four Landsat MSS bands were used to collect about 400 ground-radiance readings at each site; these values were used to compute the ground reflectances at these two sites during the satellite overflights.[1]

The dominant perennial vegetation species over most of the image area, including East Mesa, are the creosote and white bursage bushes and the big galleta grass (MacKinnon *et al.*, 1990). The many ephemeral (annual) species (grasses and various plants) are responsible for most of the seasonal biomass changes. Ground photographs and field observations indicate that vegetation in the East Mesa study area was primarily composed of creosote bushes with an areal coverage of 4 to 7 percent, which is generally too small to reduce wind erosion. The creosote bushes showed little or no change in areal coverage during our seasonal studies, although their crowns became some what denser during the spring when sufficient moisture was present. The ephemerals, on the other hand, showed great seasonal and precipitation-induced changes. The creosote bushes and other perennial species grow on both good and poor soils and rocky areas and are relatively insensitive to short-term changes in precipitation. As is shown later, the areas of poor rocky soil undergo little or no change in vegetation as detected by the satellite images. This may be due to the fact that ephemerals typically do not grow abundantly in poor soil, even if precipitation is above average.

Methods

An important step in the comparison of multitemporal remotely sensed images is geometric and radiometric calibration. In general, geometric calibration is more straightforward than radiometric calibration. In this project, image-to-image control points were used to map/slave geometrically all of the Landsat MSS data to the MSS image of 26 February 1984 (the master). The 1984 dataset was one of the first used in the project; it was selected as the geometric master at the beginning of the project, because it represents the cumulative effects of the 1983-84 El Nino. Data from most of the other years were compared with this dataset. In most cases, about 15 to 25 image control points were sufficient to give the desired geometric registration accuracy of one pixel (picture element).

Radiometric calibration is often more difficult than geometric calibration because of atmospheric effects and radiometric errors within the imaging system. There are various methods to calibrate radiometrically a digital image, depending on the information available about the sensor, atmosphere, and ground truth for the date of image acquisition (Barker, 1983; Slater, 1987; Price, 1987; Chavez, 1989; Teillet *et al.*, 1990). Without radiometric calibration, it can be more difficult to quantify and interpret changes on multitemporal images. However, many changes can be detected without applying a radiometric calibration, but, to identify automatically what the detected changes are, even in a general sense, calibration becomes critical. Depending on the application, the required calibration may be either absolute, where a digital number (DN) is converted to a ground reflectance, or relative, where the same DN in both images represents the same reflectance, regardless of what that reflectance value may be on the ground. In this project, both absolute and relative calibrations were used to develop a hybrid procedure to cali-

[1]Any use of trade or firm names in this publication is for descriptive purposes only and does not imply endorsement by the U.S. Government.

brate the historical satellite-image data. However, for comparison, the uncalibrated data were also used as input to a change-detection procedure that automatically applies a first-order, relative image-to-image calibration by removing most image-wide, low-frequency differences between the two input images.

Generally, absolute calibration is achieved by using either (1) a model that converts the DN values in an image to a ground-reflectance value or (2) ground-reflectance measurements collected during the satellite overpass and applying a brute-force matching procedure. The results indicate that relative image-to-image calibration can be used if either the percentage of total pixels whose DNs have changed in the image is small relative to the entire image, or if the overall reflectance distribution and dynamic range remain rather constant except for image-wide, low-frequency differences. Both of these conditions often exist in arid and semi-arid environments when an entire scene is used. Acceptable relative image-to-image calibration results were generated using not only a full scene but also only subareas within the scene. These subareas have relatively few changes, and not only is the DN range large, but the overall brightness distribution is quite stable.

The relative image-to-image radiometric calibration method uses a histogram-matching procedure. Histograms of the DNs within the two multitemporal images, master and slave, are computed for either the entire image or a subarea that has been selected based on either visual analysis and/or field knowledge about the area. The histograms of the master and slave images are used to identify the DN values of preselected cumulative percentage points. In this study the 1, 10, 20, 30, 40, 50, 60, 70, 80, 90, and 99 percentage points were used. The percentage sampling interval can be important, because if it is too small, such as every one or two percent, then the actual matching procedure can distort or remove some of the high-frequency differences caused by actual changes on the ground. The lower resolution sampling allows matching of the overall image brightness distribution, but not of the more local higher frequency changes within the brightness range of the histograms. Once these DN locations are found within histograms of both the master and slave images, a histogram-matching transformation is applied to the slave image so that its histogram will have the same characteristics as the master at the selected sampling interval (i.e., the same cumulative percentages occur at the same DNs). Again, in this procedure we assume that the master and slave images have the same dynamic range and DN-distribution characteristics at the given sampling intervals; we can make this assumption because the DN values of a large majority of the pixels have not changed, and, even with brightness changes on the ground, the overall brightness distribution of the entire image area remains rather stable.

Usually, in arid and semi-arid environments, the number of pixels whose DNs change significantly is statistically so small that it does not influence the overall dynamic range and distribution characteristics of the entire image or subarea being used. We tested the different datasets being used to see how robust these procedures and assumptions would be for the multitemporal pairs. In the tests, we used not only areas that changed very little between acquisitions of the two images, but also included agricultural areas where many changes did occur. For these data, even with the agricultural areas where crop rotation and growth did include substantial changes, the histogram-matching function changed very little (usually by one DN or less). The main reason for this is that, even though the DN values of some pixels were changing within the image, the overall dynamic range and distribution of the reflectances stayed rather stable, therefore affecting the histogram-matching results very little. It is important to note that two-dimensional histogram-matching is not being done; instead, the procedure is to apply a one-dimensional histogram-matching of the two images. Our assumptions will not always be valid in all environments, so this procedure must be used carefully. However, a scene-to-scene radiometric normalization technique that also uses "approximately constant reflectivities for the viewing conditions" has been employed to look at land-use changes in non-arid environments (Schott *et al.*, 1988). These authors concluded that changes in reflectance of more than one percent could be correctly detected.

At times, absolute calibration is preferred, and it is required for the part of our project that will need physical units to compute dust volumes from changes in optical thickness. Absolute calibration can also be critical when working with data covering more than two dates and/or data collected by different sensors. Because of these requirements, we developed a hybrid procedure that allows an absolute calibration to be applied to historical multitemporal data by using radiance data collected in the field rather than by using a modeling procedure. The hybrid is made by merging the brute-force, absolute-calibration method that uses ground radiances collected during a recent satellite overpass and the relative image-to-image histogram-matching calibration procedures. In the hybrid procedure, ground-radiance measurements, collected in the field over dark and bright targets during the 1992 Landsat MSS overpass, were used to apply an absolute calibration (using the brute-force matching procedure) to the Landsat MSS data collected during the overpasses; these data become the radiometric master. We used the relative image-to-image histogram-matching calibration procedure in which an absolute calibration is applied to the historical Landsat MSS slave image (i.e., it maps the slave image onto the absolute radiometrically calibrated master). This method was used instead of a modeling procedure because of errors that can be present in models due to (1) insufficient atmospheric information for the dates of the historical data being used, and (2), even if atmospheric information is available, the model may not be correct because other errors are still present. These two problems can be avoided by using the hybrid method, realizing that the two assumptions will not always be valid in all environments. This procedure allows us to apply an absolute calibration to historical or new images using radiance data collected in the field on a date that corresponds to the date of the image being used as the radiometric master. The procedure is useful, because most multitemporal studies use images collected before the studies are begun.

Calibration is often critical but can be difficult to apply. Fortunately, there is a change-detection procedure that can be used with uncalibrated data, because it automatically applies a first-order, relative image-to-image calibration. Gunther (1982) and, later, Chavez and Kwarteng (1989) showed that principal component analysis (PCA) can be used to map information that is unique between two images. The procedure called selective PCA was used to map the spectral contrast between Landsat Thematic Mapper bands (Chavez and Kwarteng, 1989). In other previous studies, change-detection has been done by using (1) image difference, (2) ratioing of the image data collected at two different times, or (3) a post-classification difference (Chavez *et al.*, 1977; Singh, 1989). Artifacts can result from the image difference or ratio-

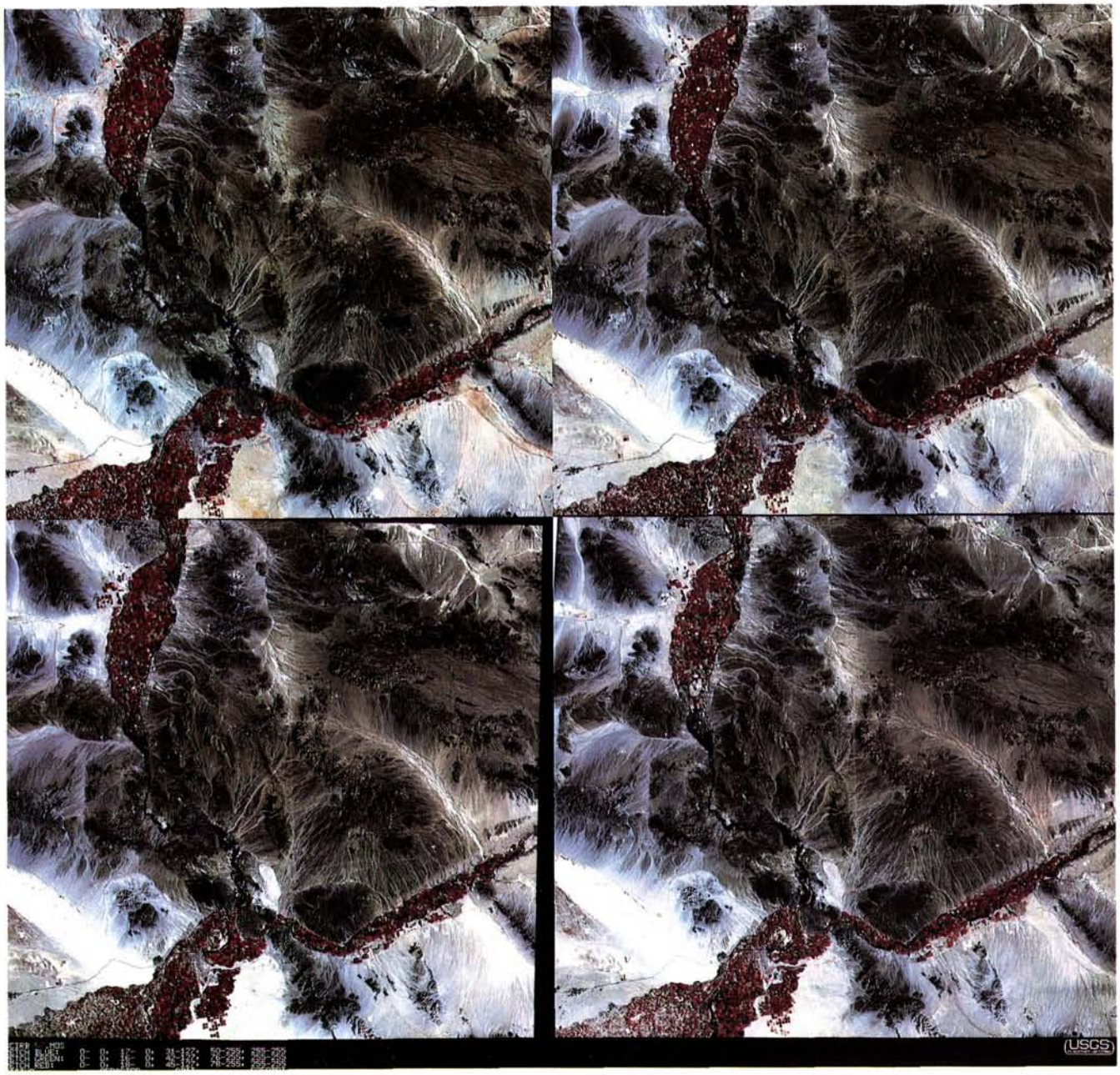

Plate 1. False-color composites of four Landsat MSS images used in the study, made by using MSS bands 4, 5, and 7 in the blue, green, and red color filters, respectively. Acquisition dates are 4 April 1992 (upper left), 1 July 1992 (upper right), 24 February 1981 (lower left), and 26 February 1984 (lower right). The images have been geometrically and radiometically calibrated to the master Landsat MSS image; for visual display and comparison, the same contrast stretch has been applied to all four. The Gila River is at the bottom of the images and joins the Colorado River in the lower left. Also in the lower left is the bright area of the Algodones Dune Field, about 25 km west of Yuma. North at top; images about 185 km on a side.

ing procedures if image-wide, low-frequency differences are present in the data, such as atmospheric effects (i.e., if the data have not been calibrated). With post-classification differencing, the results can have errors due to errors in the actual classification. In this project, good results were obtained with the simple image difference, because both the relative and the hybrid image-to-image histogram-matching calibration procedures removed the image-wide, low-frequency differences. However, good change-detection results were also generated from uncalibrated data by the selective PCA procedure developed by Chavez to map spectral contrast or differences in Landsat Thematic Mapper (TM) data. The procedure

20 March 1992

1 July 1992

4 April 1992

1 July 1992

4 April 1992

1 July 1992

20 March 1992

1 July 1992

Plate 2. Vegetation cover at four locations at approximate time of Landsat and GOES overpasses of 4 April 1992 and 1 July 1992. Photographs on the left taken 4 April and 20 March (as noted), during the wet season. Photographs on the right taken 1 July 1992 during the dry season. Photograph locations within the Landsat MSS image are shown in Figure 4a.

isolates information that is unique to either of the input datasets (Chavez and Kwarteng, 1989). This is done by using only two images/bands as input rather than all bands, as is the case with standard PCA. This maps the information that is unique to each of the two images/bands to a single component (i.e., spectral contrast if two bands taken at the same time are used as input, and temporal contrast if the same bands taken at different times are used as input). Using selective PCA with only two single-band images as input at any given time makes the interpretation easier and more straightforward, because the information that is common to both images will be mapped to the first component, and information that is unique to either image will be mapped to the second component (Chavez and Kwarteng, 1989). One of the major benefits of using only two bands as input to PCA is that the procedure will automatically eliminate most image-wide, low-frequency differences between the two images (i.e., it automatically does a first-order, relative image-to-image calibration). This calibration occurs because the multiplicative and additive coefficients computed for the eigen vectors to translate (rotate and scale) the image data into the new coordinate system remove most of the major low-frequency difference between the two images. A large percentage of the image-wide, low-frequency difference between two multitemporal images will be due to atmospheric and sensor calibration differences. However, because other relatively low frequencies can affect the rotation, it is possible that an optimal image-to-image relative calibration will not be applied.

If the data have been calibrated, a simple difference of the two images involved will generate results as good as or better than those generated by the selective PCA procedure, because the image-wide low frequencies will be removed by the calibration procedure (e.g., matching of the image histograms). If the images have not been calibrated, low-frequency differences will be present in the simple difference results, which presents a problem if more than two dates are used in the multitemporal analysis, as is the case in this project. For applications requiring absolute calibration, the simple difference with the hybrid calibration procedure is the preferred method. However, if calibration is not applied, then selective PCA is preferred to simple difference.

Discussion

Most of the foregoing has dealt with the methods used to detect changes in remotely sensed data. However, just as important are the image data that are used as input to the change-detection procedure (i.e., if the information of interest is not contained in the data being analyzed, the change-detection procedure is irrelevant). Of course, the data to be used as input for change detection should be dependent on the type of changes that is of interest. In our case, as in many global-change research projects that use remotely sensed images, the changes of interest are changes in vegetation. The most widely used data product in studying vegetation with remotely sensed images is the Normalized Difference Vegetation Index (NDVI). Studies using the NDVI and other vegetation indexes are varied and include those involved with local, regional, and global mapping (Townshend and Justice, 1986; Choudhury and Tucker, 1987; Jackson and Huete, 1991; Justice *et al.*, 1991; Tucker *et al.*, 1991).

In this study, a calibrated visible band was better than the NDVI image for detecting vegetation changes in this arid to semi-arid environment (the red spectral band was the best, but the green band also generated similar results). Previous researchers who have worked with the visible and near-infrared spectral bands in their analyses have reported similar findings. In an analysis of range conditions in the Kalahari Desert of Botswana, Ringrose and Matheson (1991) found that, for low and medium vegetation densities, the red band (MSS 5) gives the best results for mapping green leaf cover. They found that vegetation indexes do not predict green leaf cover in areas of low and medium vegetation densities; however, both the red band and vegetation indexes do predict the leaf cover in high vegetation-density areas. Also, in a separate study to map sparsely vegetated rangelands, only the red band (MSS 5) was used to generate maps showing the percentage of vegetation cover (Graetz *et al.*, 1988). Perhaps one reason why the calibrated red band is better than the NDVI for detecting vegetation changes in arid and semi-arid environments is that the soils supporting most of the vegetation (grasses) have a relatively high reflectance in both the visible and near-infrared spectral bands. Therefore, the NDVI values will not change much, because the near-infrared reflectance for the soils is high, and when vegetation, which also has a high near-infrared reflectance, does grow, the change in brightness of the near-infrared band will be minimal (i.e., the near-infrared reflectance of a ground resolution cell/pixel will be high whether it is covered by bright soils or by vegetation). However, in the visible spectral bands, vegetation has a much lower spectral reflectance than it does in the near-infrared band. Therefore, it has a high spectral contrast with the bright soils in the visible part of the spectrum. Because the reflectance of vegetation in the visible/red spectral band is lower than that of the bright soils, the brightness or DN value of a pixel changes more in the red band than in the near-infrared band as vegetation covers of progressively higher densities are imaged. This observation is similar to that seen in an assessment of the conditions of mesquite and grass vegetation by McDaniel and Haas (1982). They found that the near-infrared bands (MSS 6 and 7) did not vary as much seasonally as the visible bands (MSS 4 and 5). This, combined with the fact that the ratioing process required to compute most vegetation indexes enhances random and uncorrelated noise, indicate that an individual red spectral band can be more efficient than vegetation indexes in detecting vegetation changes in arid and semi-arid environments.

Results

Our results were generated from three different pairs of multitemporal satellite images. The three pairs show vegetation changes in the same desert area in the southwestern United States.

Landsat MSS Images Acquired on 4 April 1992 and 1 July 1992

Ground radiances were measured in the field during these overpasses, both to use in absolute calibration and to provide ground truth about the extent of the vegetation cover. As described earlier, this pair of images shows conditions during a very wet season and the following dry season. On these two dates and on one in mid-March, we observed the vegetation growth cycle at selected sites within the image area. The photographs that we took to show the extent of the vegetation cover at several locations within the southwest quadrant of the full MSS scenes are shown in Plate 2. Note that the areas where the ground photographs were taken show very little red in the color-infrared composites shown in Plate 1, indicating that very little vegetation existed at these locations. The calibrated MSS band-5 images are shown in Figure 1 and the change image of Figure 2 clearly shows changes in different areas within the full scene, including the lower left

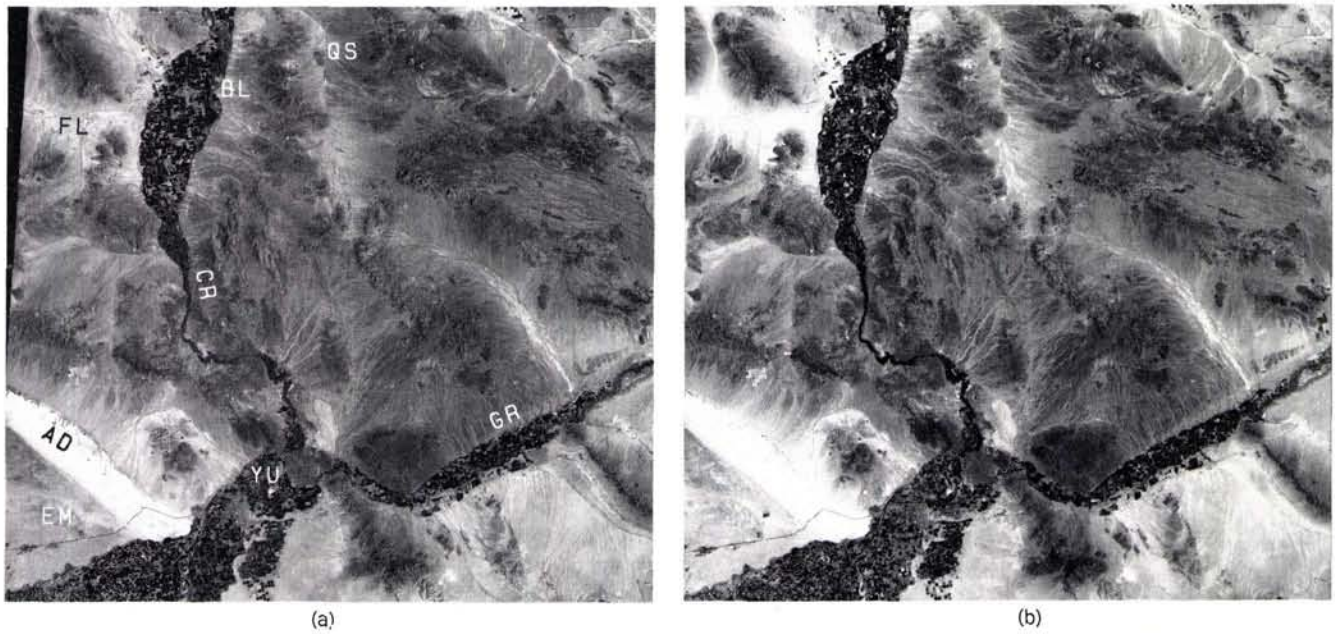

(a) (b)

Figure 1. Full-scene, calibrated Landsat MSS band 5 (red spectral band) image acquired on 4 April 1992 (a) and 1 July 1992 (b). They have been geometrically and radiometrically calibrated so that the same DN represents the same ground reflectance. For comparison, the same contrast stretch has been applied to each image. EM, East Mesa; AD, Algodones Dunes; YU, Yuma; GR, Gila River; CR, Colorado River; FL, Ford Dry Lake; BL, Blythe; and QS, Quartzsite.

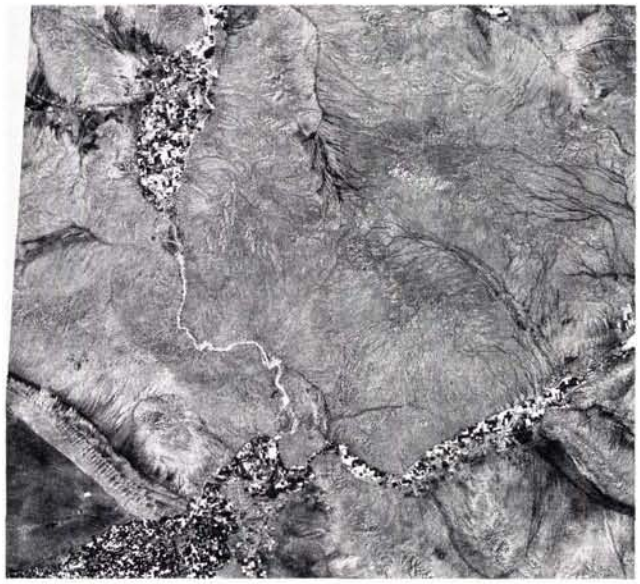

Figure 2. Change image generated from the images shown in Figure 1 by a simple difference procedure. The dark areas had more actively growing vegetation in April than in July. The bright areas had more vegetation in July than in April. This figure shows changes that occur within the same year between a wet (spring) and dry (summer) season.

quadrant of the image, where the ground photographs were taken. Note that changes in the heavily vegetated agricultural areas are also readily detected by the change-detection procedure that used the calibrated Landsat MSS band 5 data. This implies that perhaps the use of the red band (MSS 5) with the given change-detection procedure may also be useful in highly vegetated areas.

To emphasize the relatively low density of vegetation in this area, as shown by the absence of red in the color composite in Plate 1, the NDVI images for this subarea are shown in Figure 3. Note their absence of detail as compared with the calibrated MSS band 5 data (Figure 4). As shown in Figure 5, the calibrated MSS band 5 change image shows more vegetation changes than the NDVI data. The ground photographs (Plate 2) indicate that vegetation changes did indeed occur from April to July of 1992 in this area of low vegetation density. The field of cultivated jojoba shrubs (large bright rectangle) exemplifies the increase in vegetation. (At this scale, we can see that in the Algodones Dune Field some of the effect of shadow-length differences between the April and July images are being detected.)

Landsat MSS Images Acquired on 24 February 1981 and 26 February 1984

The 1981 data represent a dry year; the 1984 data, a wet year (El Nino began in December 1982 and continued through January 1984). Both images of Figure 6 were obtained at the beginning of the season of natural vegetation growth in early Spring, and thus they may not show the full growth achieved during their respective seasons. Because these data were collected well before the start of this project, as is often the case in multitemporal studies, the hybrid calibration method was used. The change image generated from these two radiometr-

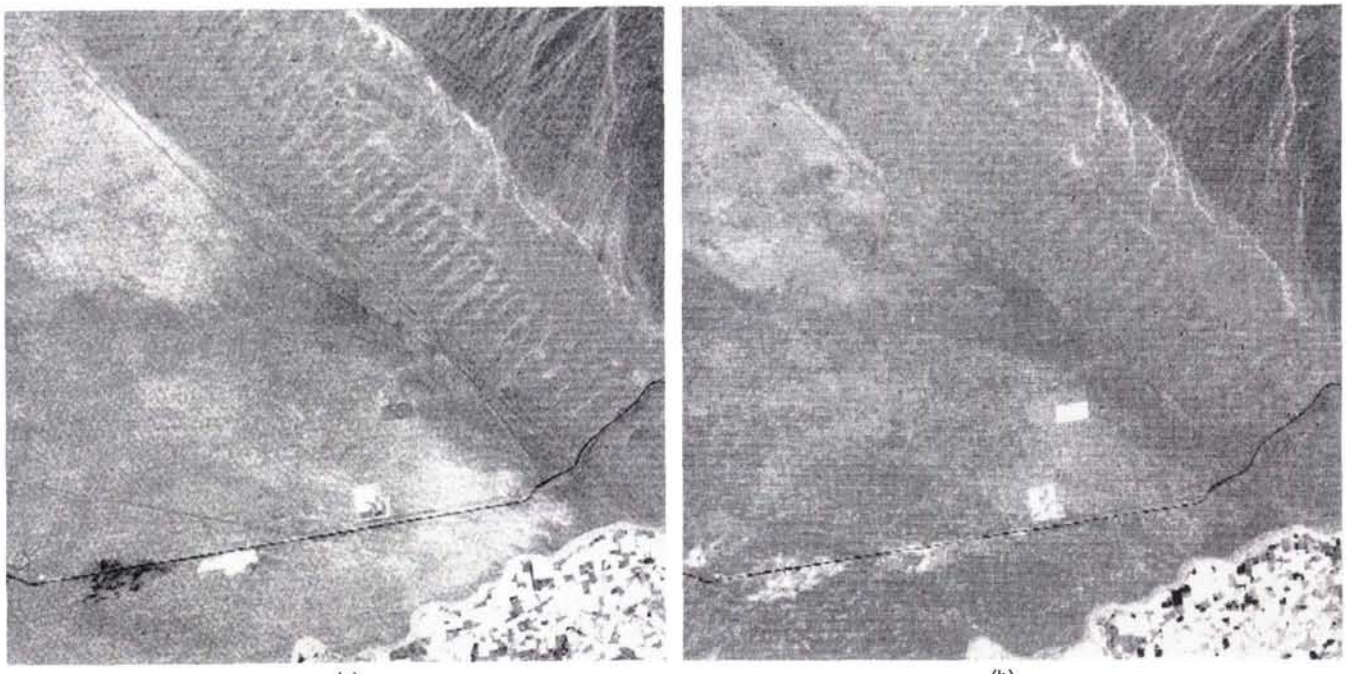

(a) (b)

Figure 3. Landsat MSS NDVI images for the subarea shown in Figure 4. (a) Image acquired 4 April 1992. (b) Image acquired 1 July 1992. Both images were generated from the calibrated Landsat MSS data. The most dramatic differences in vegetation cover can be seen in the agricultural areas in the lower right portion of the images, but few differences can be seen at the locations of the ground photographs in Plate 2 (see locations given in Figure 4).

ically calibrated images is shown in Figure 7. As in the previous example, a simple differencing procedure was used, because the data were calibrated by the hybrid procedure. Note that some of the locations of vegetation change are the same as those shown in Figure 5a. However, several locations do not show the vegetation changes seen in the 1992 data, including the East Mesa site west of the Algodones Dunes. Possible reasons for this difference are the varied spatial distribution of rainfall between the four dates of image acquisition and the difference between vegetation in late February (early part of the wet season) and early April (latter part of the wet season). Field information and ground photographs during these satellite overpasses are not available for comparison. However, photographs were taken earlier (MacKinnon *et al.*, 1990) at a nearby location shown in the lower center of the images (E in Figure 6a). These photographs show that the vegetation cover in 1984 was more extensive than in 1981.

GOES VISSR Images Acquired on 4 April 1992 and 1 July 1992

Because dust storms can be detected with GOES VISSR images (MacKinnon and Chavez, 1993), and because, as shown here, the visible/red band is a better tool than the NDVI for detecting vegetation changes in the desert, we were curious to find out if vegetation changes could be detected by using GOES VISSR images. The GOES VISSR images that we used (Figure 8) were acquired on the same dates as the images used in the first Landsat MSS comparison, when we were in the field collecting ground-radiance information. This allowed us to compare all three datasets. Typically, in regional and global vegetation mapping projects, AVHRR data are used. One of the advantages of the AVHRR data is that, unlike the VISSR, the AVHRR data have the near-infrared spectral band to compute the NDVI. However, in our work this was not a problem, because a calibrated visible/red band is better than the NDVI for detecting vegetation changes. A second disadvantage of the VISSR images is that their radiometric quality is relatively poor; they have a lower radiometric range, less sensitivity, and a lower signal-to-noise ratio than AVHRR images. However, a major advantage of the VISSR data over the AVHRR is that they do not have the radiometric and geometric problems caused by the large-view-angle geometry of the AVHRR system. The VISSR view-angle characteristics are similar to those of Landsat because of its much higher altitude (approximately 35,800 km compared with 860 km for AVHRR). Another advantage of VISSR over AVHRR is that its temporal frequency/coverage is better.

The fact that a GOES VISSR image is acquired every 30 minutes can be used to help solve the problem of its lower radiometric dynamic range and relatively poor radiometric quality. We solved this problem by digitally registering and merging VISSR images taken with a relatively higher temporal frequency (hours/days) than the temporal frequency (months/years) of the image data being used to detect changes. We then generated a radiometrically improved VISSR image by summing the digitally registered and merged images. (The average rather than the sum can be used if one wants the data range to stay within the 8-bit range of 0 to 255.) The VISSR images used to generate the sum image can be collected either on the same day or at the same time of day

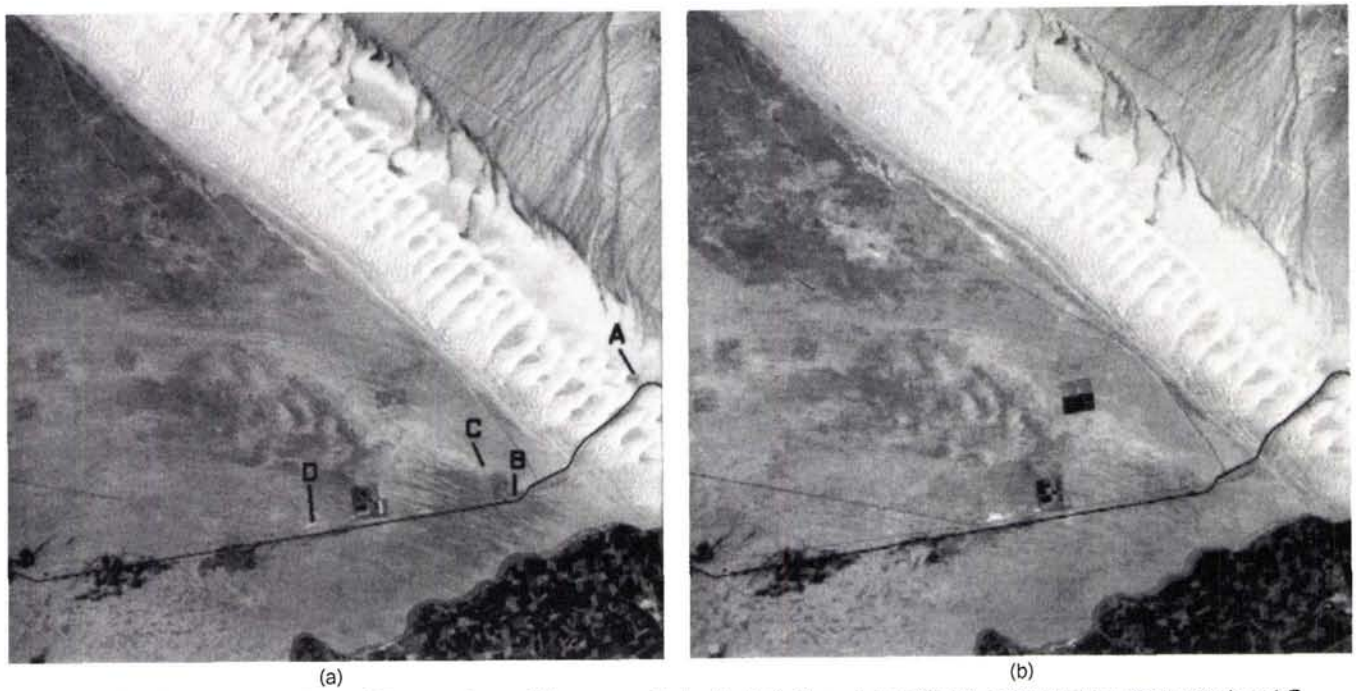

(a) (b)

Figure 4. Southwestern portions of Figures 1a and 1b, respectively (April (left) and July (right) calibrated Landsat MSS band 5 data). Images are enlarged to show the Algodones Dunes in greater detail. The locations of the ground photographs shown in Plate 2 are indicated in Figure 4a. The dark line near the bottom of the images is the All-American Canal. Many of the differences between the images are related to vegetation growth along the drainages and in flat open areas where fine-grained sediments had been deposited.

within a few days of one another. Of course, the images must be geometrically registered to one another, but with the narrow Landsat-type viewing angles, this is not a major problem. In our study, morning and afternoon VISSR images for 4 April and 1 July 1992 were added to create the two VISSR sum images to use as input to the change-detection procedure. Because these dates are the same as the dates of acquisition of the Landsat MSS images and of our ground radiances and photographs, both the Landsat MSS and ground information served as ground truth for the results generated from the GOES VISSR images. Ideally, to improve the signal-to-noise ratio further, more images that are temporally very close to one another would be used to create the GOES VISSR sum images (e.g., all the 9:30 AM GOES VISSR images for the first week in April versus all the 9:30 AM images for the first week in July). The user may want to consider working with the 8:30 AM or earlier images in July to keep the sun-elevation angles about the same. However, application of either the hybrid or the relative image-to-image calibration procedure will minimize the need for this type of temporal shift. The following sequence was used to generate the change image from GOES VISSR data:

- Geometrically registering the VISSR sub images to the spatially compressed and radiometrically calibrated Landsat MSS images.
- Creating the VISSR sum/average images by using the AM and PM pairs for April and July. (A full week-long set of images will be used in the future.)
- Appling the hybrid image-to-image radiometric calibration to the GOES VISSR sum images by using the compressed calibrated Landsat MSS images as the radiometric masters. (Note that this step is not required if only change detection is desired, because the PC2 of the selective PCA between the two images would generate a visually similar change image.)
- Using simple differencing to generate the VISSR change image between the calibrated sum images of April and July.
- Appling a small, 5- by 5-pixel smoothing filter to the resulting change image to improve the signal-to-noise ratio further. This step may not be needed if more VISSR images are used to generate the sum images, that is, to generate the sum image by using five or seven days of images rather than just two images for one day.

Because the GOES VISSR sum images were radiometrically calibrated to the resampled, coarser resolution, Landsat MSS images that were radiometrically calibrated and acquired on the same date, the same amount of DN change in the GOES VISSR data will represent close to the same amount of change in the Landsat MSS data. The changes are approximate because there will be small errors in the absolute reflectance sense; these errors will arise because the spectral wavelengths for the visible bands being used are not identical on the GOES VISSR and Landsat MSS systems. (The visible GOES VISSR band covers the 0.55- to 0.70-micrometre spectral window; the Landsat MSS red spectral band covers the 0.60- to 0.70-micrometre window). To get a better spectral window match, the Landsat MSS bands 4 and 5 can be used to generate a weighted sum band that simulates the VISSR spectral window more accurately. The calibrated GOES VISSR images generated from the sum images for 4 April and 1 July 1992, respectively, are shown in Figures 8a and 8b.

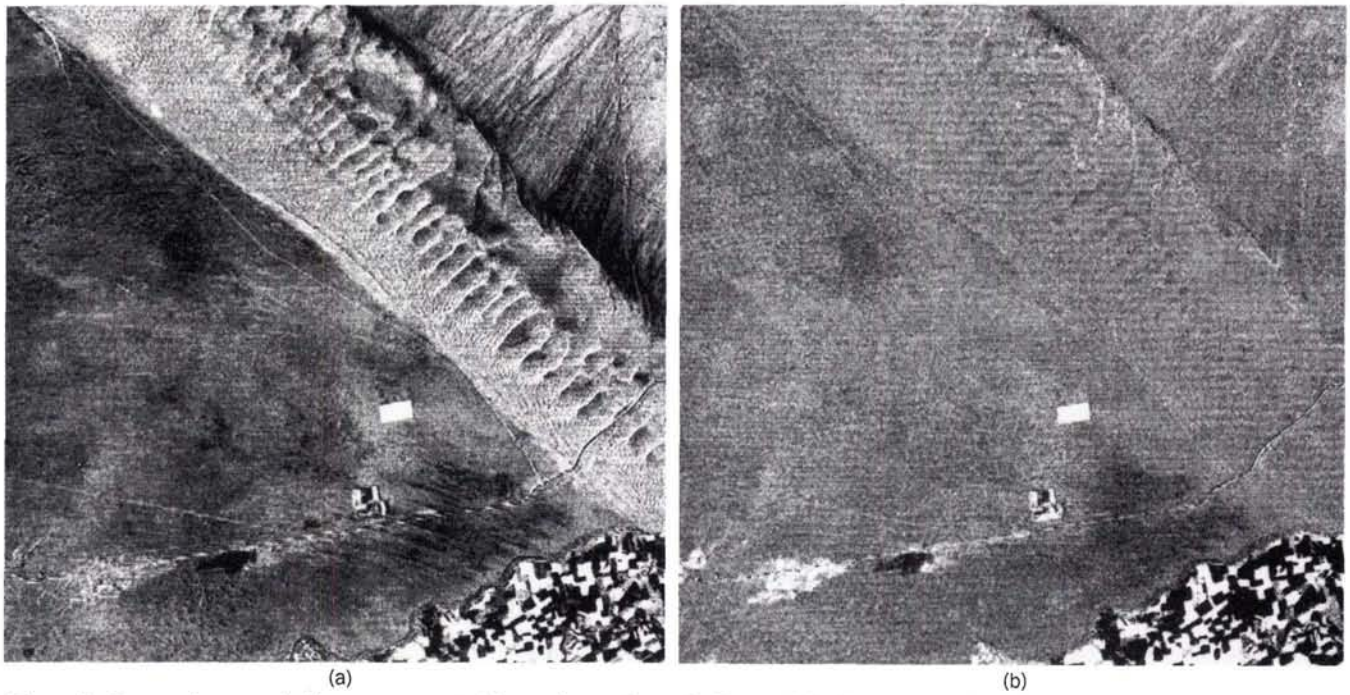

(a) (b)

Figure 5. Change images. (a) Image generated from those shown in Figure 4 (calibrated Landsat MSS band 5). (b) Image generated from those shown in Figure 3 (Landsat MSS NDVI). In both images, dark areas had more actively growing vegetation in April than in July. Bright areas had more vegetation in July than in April; an example is the field of jojoba shrubs shown as the large bright rectangle. Note both the larger number and the larger amplitude of changes detected by the calibrated Landsat MSS band 5 than by the NDVI product.

The change images generated from the GOES VISSR and compressed Landsat MSS data are shown in Figure 9. Generally, the correlation is good between the patterns in the two change images; some of the differences that do exist are due to the difference in spatial resolution between the two original datasets. For example, the differences seen by the Landsat MSS in agricultural fields may not be seen as well in the GOES VISSR data, because the radiometric changes are occurring on a relatively high spatial frequency on the ground; this can cause positive and negative changes to average each other out in the lower resolution pixel of the GOES VISSR data. Because most of the natural vegetation changes result from the growth cycle of ephemerals, which generally cover a relatively large area, these changes have a lower frequency spatial pattern than do changes in agricultural areas. Note that a first-order, cloud-removal technique can be used during the summing of the images to improve the resultant image. (The cloud-removal technique would eliminate pixels whose DN values differ from the medium or cloud-free DN values by a selected threshold).

Summary

We have detected changes in natural vegetation in the arid to semi-arid desert of the southwestern United States using Landsat MSS and GOES VISSR multitemporal images. Calibration is very important if automatic identification of the changes is desired, and if more than two dates will be compared. However, the use of selective PCA on uncalibrated images will allow the automatic detection of changes. Our hybrid method allows us to apply an absolute calibration to historical data by using recent field information rather than a modeling procedure. In this study, the calibrated red spectral band was found to be a better dataset to detect changes in arid and semi-arid environments than the widely used NDVI. This implies that groups who are generating regional and global databases from remotely sensed images, such as from AVHRR, for use in global-change research should make sure that the visible bands, the red band in particular, are included as part of their data bases along with the NDVI.

Some of the detected changes occurred in areas where the standard Landsat MSS false-color composite and the MSS NDVI indicated that the vegetation density was relatively low. However, our field studies made at the time of two of the Landsat MSS and GOES VISSR overpasses show that vegetation was indeed present (Plate 2) and that vegetation changes in areas with relatively low vegetation density can be detected. Note that by mapping areas where natural vegetation does fluctuate, our procedure is also indirectly mapping areas of soils that will support vegetation if rainfall is sufficient. The procedure also generates information that may be useful to identify soils vulnerable to wind erosion and desertification, as well as information on possible grazing locations. By showing that the red/visible band can be used to detect vegetation changes, and by using the sum of several same-date or same-time-of-day GOES VISSR images to generate a GOES VISSR image with improved radiometric signal-to-noise, we have demonstrated that these readily available data can be used for some regional and global mapping applications. These

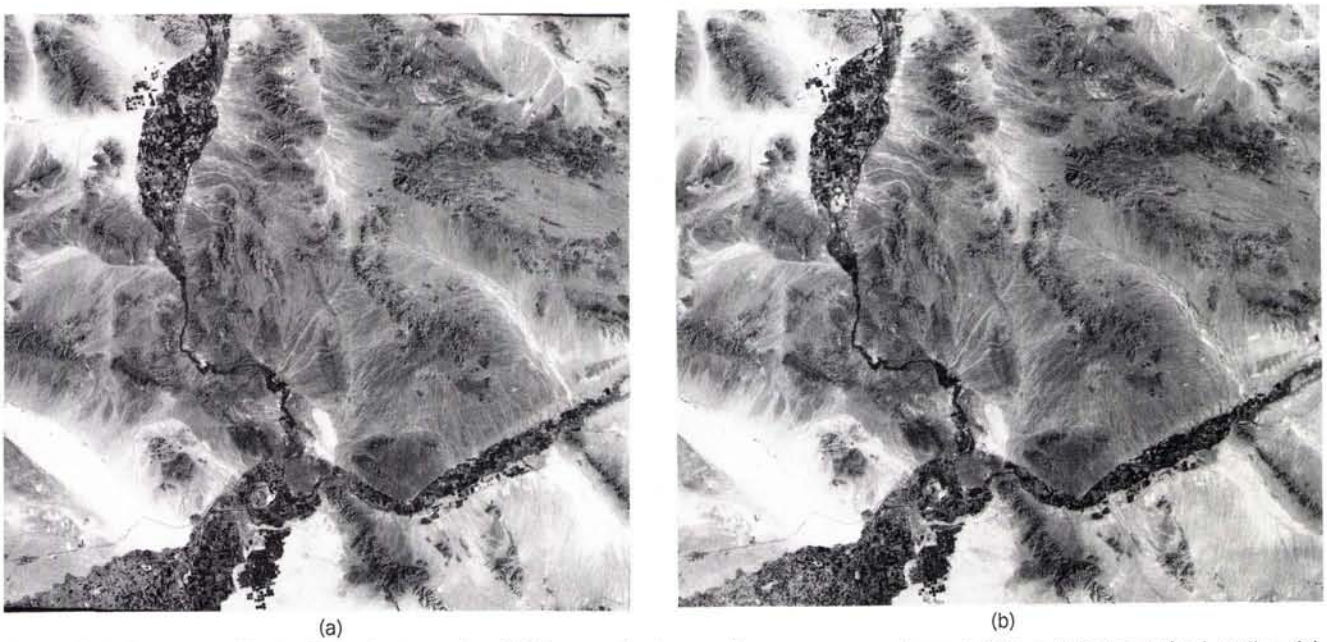

(a) (b)

Figure 6. Full-scene calibrated Landsat MSS band 5 images that cover the same area shown in Figure 1 but acquired earlier. (a) Image acquired 24 February 1981. (b) Image acquired 26 February 1984. Image (a) was calibrated to the master (image b). The same stretch was applied to both images as was given the image acquired on 1 July 1992 (Figure 1b), so that changes could be noted between (a) and (b) of Figure 6, between (a) and (b) of Figure 1, or between any pair of the four images. The letter E in Figure 6a identifies the approximate location of the ground photograph in MacKinnon *et al.* (1990; see text).

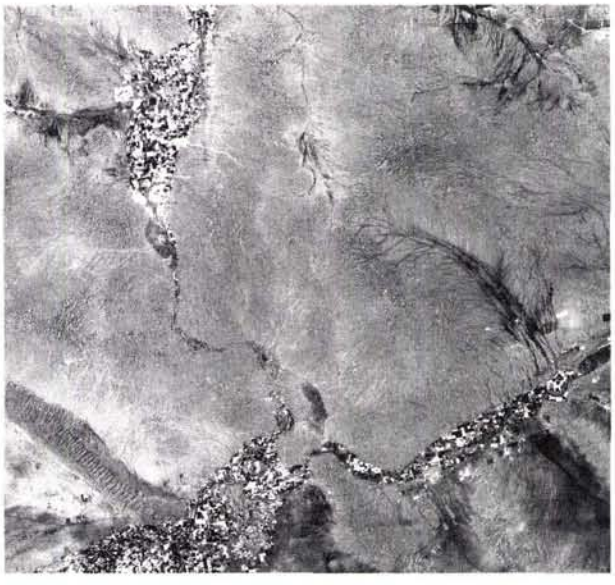

Figure 7. Change image generated from the images shown in Figure 6 by a simple differencing procedure. Here, the dark areas were more vegetated in 1984 than in 1981; the bright areas were more vegetated in 1981 than in 1984. This figure indicates changes that occurred at the same time of the year between dry (1981) and wet (1984) years.

data will not have the geometric and radiometric problems encountered with the widely used AVHRR images because of the much narrower view-angle geometry. (The view-angle geometry is similar to that of Landsat.) Also, the temporal frequency coverage of the GOES VISSR data is even higher than the AVHRR, so it will be better suited for some multitemporal analyses.

Acknowledgments

This project was funded by the National Aeronautics and Space Administration (NASA) through contract NRA91-OSSA-07. We would like to thank Stuart Sides for his help with the radiometers and collection of the field radiances. Also, we thank Miguel Velasco and Rosendo Gonzalez for help with processing the Landsat MSS and GOES VISSR images.

References

Barker, J., 1983. Relative radiometric calibration of TM reflective bands, *Landsat-4 Science Characterization Early Results*, NASA Conference Publication 2355, III:1–29.

Chavez, P.S., Jr., 1989. Radiometric calibration of Landsat Thematic Mapper Multispectral images, *Photogrammetric Engineering & Remote Sensing*, 55(9):1285–1294.

Chavez, P.S., Jr., G.L. Berlin, and W.B. Mitchell, 1977. Computer enchancement techniques of Landsat MSS digital images for land use/cover assessments, *Proceedings of the Sixth Remote Sensing of Earth Resources Symposium*, Tullahoma, Tenn., pp. 259–275.

Chavez, P.S., Jr., and A.Y. Kwarteng, 1989. Extracting spectral contrast in Landsat Thematic Mapper image data using selective principal component analysis, *Photogrammetric Engineering & Remote Sensing*, 55(3):339–348.

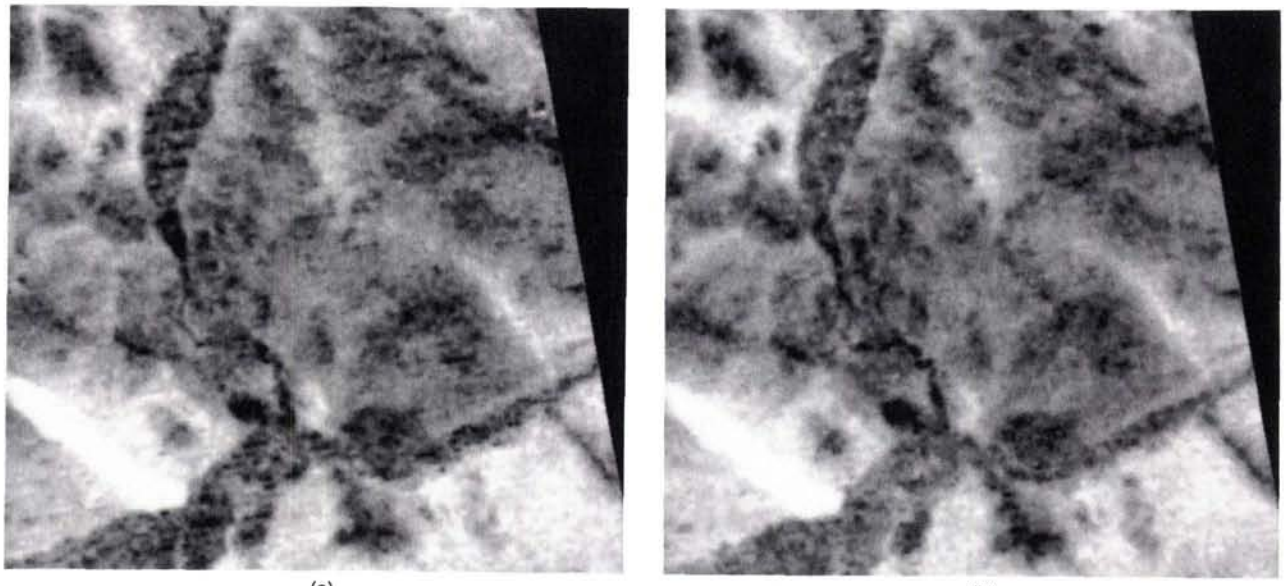

(a) (b)

Figure 8. GOES VISSR images generated by geometrically registering them to the compressed and calibrated Landsat MSS band 5 images, summing the morning and afternoon VISSR images, and then matching the DN histogram of the summed images to the calibrated Landsat images. (a) Data acquired 4 April 1992. (b) Data acquired 1 July 1992. The area covered is about the same as that of the Landsat MSS images; spatial resolution is about 1 km. For visual display and comparison, the same contrast stretch that was used on the Landsat images shown in Figures 1 and 6 was applied to these two images.

Choudhury, B.J., and C.J. Tucker, 1987. Satellite observed seasonal and inter-annual variation of vegetation over the Kalahari, the Great Victoria Desert, and the Great Sandy Desert: 1979–1984, *Remote Sensing of Environment*, 23:233–241.

Gillette, D.A., and K.J. Hanson, 1989. Spatial and temporal variability of dust production caused by wind erosion in the United States, *Journal of Geophysical Research*, 94(D2):2197–2206.

Fung, T., 1990. An assessment of TM imagery for land-cover change detection, *IEEE Transactions on Geoscience and Remote Sensing*, 28(4):681–684.

Graetz, R.D., R.P. Pech, and A.W. Davis, 1988. The assessment and monitoring of sparsely vegetated rangelands using calibrated Landsat data, *International Journal of Remote Sensing*, 9(7):1201–1222.

Gunther, F.J., 1982. A new principal components procedure to aid the analysis of Landsat MSS digital data, *Proceedings IEEE Computer Society Conference on Pattern Recognition and Image Processing*, 14–17 June 1982, Las Vegas, Nevada, pp. 38–43.

Jackson, R.D., and A.R. Huete, 1991. Interpreting vegetation indices, *Preventive Veterinary Medicine*, 11:185–200.

Jensen, J.R., and D.L. Toll, 1982. Detecting residential land-use development at the urban fringe, *Photogrammetric Engineering & Remote Sensing*, 48(4):629–643.

Justice, C.O., J.R.G. Townshend, and V.L. Kalb, 1991. Representation of vegetation by continental data sets derived from NOAA-AVHRR data, *International Journal of Remote Sensing*, 12(5):999–1021.

MacKinnon, D.J., and P.S. Chavez, Jr., 1993. Dust storms, *Earth*, 2(3):60–65.

MacKinnon, D.J., D.F. Elder, P.J. Helm, J.F. Tuesink, and C.A. Nist, 1990. A method of evaluating effects of antecedent precipitation on dust storms and its application to Yuma, Arizona, 1981–1988, *Climatic Change*, 17:331–360.

Pewe, T.L., 1981. Desert dust: an overview, *Desert Dust: Origin, Characteristics, and Effect on Man* (T.L. Pewe, editor), Geological Society of America Spec. Pap. 186, pp. 1–10.

McCauley, J.F., C.S. Breed, M.J. Grolier, and K.J. MacKinnon, 1981. The U.S. dust storm of February 1977, *Geological Society of America Spec. Pap. 186*, pp. 123–147.

McDaniel, K.C., and R.H. Haas, 1982. Assessing mesquite-grass vegetation condition from Landsat, *Photogrammetric Engineering & Remote Sensing*, 48(3):441–450.

Price, J.C., 1987. Calibration of satellite radiometers and the comparison of vegetation indices, *Remote Sensing of Environment*, 21:15–27.

Raupach, M.R., D.A. Gillette, and J.F. Leys, 1993. The effect of roughness elements on wind-erosion threshold, *Journal of Geophyical Research*, 98:3023–3029.

Ringrose, S., and W. Matheson, 1991. A Landsat analysis of range conditions in the Botswana Kalahari drought, *International Journal of Remote Sensing*, 12(5):1023–1051.

Robinove, C.J., P.S. Chavez, Jr., D. Gehring, and R. Holmgrem, 1981. Arid land monitoring using Landsat albedo difference images, *Remote Sensing of Environment*, 11:133–156.

Schott, J.R., C. Salvaggio, and W.J. Volchok, 1988. Radiometric scene normalization using pseudoinvariant features, *Remote Sensing of Environment*, 26:1–16.

Shepard, J.R., 1964. A concept of change detection, *Proceedings 30th Annual Meeting of the American Society of Photogrammetry*, Washington D.C., 17–20 March 1964, pp. 648–651.

Singh, A., 1989. Review article: Digital change detection techniques using remotely-sensed data, *International Journal of Remote Sensing*, 10(6):989–1003.

Slater, P.N., 1987. Reflectance and radiance based methods for the in-flight absolute calibration of multispectral sensors, *Remote Sensing of Environment*, 22:11–37.

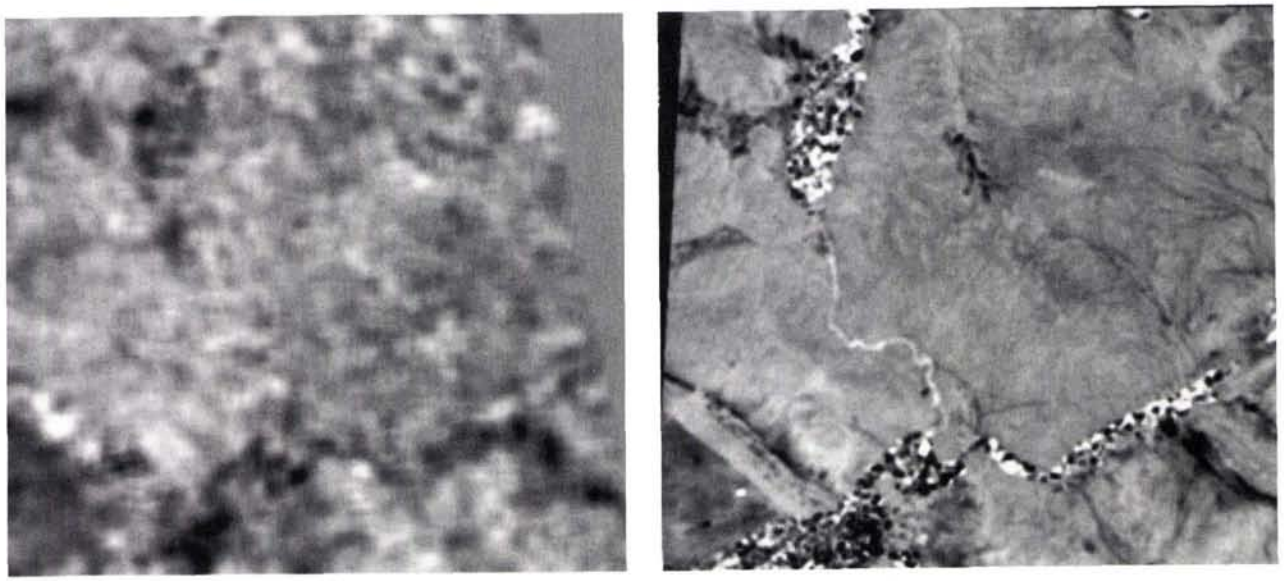

(a)

Figure 9. Contrasting change images. (a) Image generated from the two GOES VISSR images shown in Figure 8 by the simple difference procedure. (b) Difference image generated from Landsat MSS data acquired on the same dates. This image was digitally compressed and smoothed to generate a product that has a closer spatial resolution to the GOES VISSR data than the one shown in Figure 2. The general patterns of the vegetation changes shown in both images are similar. The dark areas had more vegetation during April than during July; the reverse is true for the bright areas.

Teillet, P.M., P.N. Slater, Y. Ding, R.P. Santer, R.D. Jackson, and M.S. Moran, 1990. Three methods for the absolute calibration of the NOAA AVHRR sensors in-flight, *Remote Sensing of Environment*, 31:105–120.

Townshend, J.R.G., and C.O. Justice, 1986. Analysis of the dynamics of African vegetation using the normalized difference vegetation index, *International Journal of Remote Sensing*, 7(11):1435–1445.

Tucker, C.J., W.W. Newcomb, S.O. Los, and S.D. Prince, 1991. Mean and inter-year variation of growing-season normalized difference vegetation index for the Sahel 1981–1989, *International Journal of Remote Sensing*, 12(6):1133–1135.

UCAR (University Corporation for Atmosphereic Research), Office for Interdisciplinary Earth Studies, 1991. *Report on Arid Ecosystems Interactions Workshop*, Report OIES-6, Boulder, Colo., 81 p.